8-2009

X-Ray Particle Tracking Velocimetry in Fluidized Beds

Joshua B. Drake
Iowa State University

Lie Tang
Iowa State University, lietang@iastate.edu

Theodore J. Heindel
Iowa State University, theindel@iastate.edu

X-Ray Particle Tracking Velocimetry in Fluidized Beds

Abstract
Fluidized beds are commonly found in the chemical and energy processing industries because of their low pressure drop, uniform temperature distribution, and high heat transfer rates. For example, in biomass gasification, biomass particles are injected into a heated bubbling bed of inert material (typically refractory sand) that volatilizes to form a flammable gas. However, the movement of the biomass particle through the bubbling bed is difficult to quantify because the systems are opaque. This paper describes X-ray particle tracking velocimetry (XPTV) applied to fluidized beds, where X-ray flow visualization is used to track the location of a single fabricated tracer particle as a function of time in a fluidized bed to study the bed/particle hydrodynamics. Using stereoscopic X-ray imaging, the 3D position of the tracer particle as a function of time is determined, from which tracer particle velocity can be calculated. Details and challenges of the XPTV process are also summarized.

Keywords
Agricultural and Biosystems Engineering, fluidized bed, particle tracking, stereography, x-rays, x-ray particle tracking velocimetry

Disciplines
Acoustics, Dynamics, and Controls | Biomechanical Engineering | Biomedical Engineering and Bioengineering | Fluid Dynamics

Comments
This is a conference proceeding from *ASME 2009 Fluids Engineering Division Summer Meeting* 1 (2009): 1733, doi:10.1115/FEDSM2009-78150. Posted with permission.

Proceedings of the ASME 2009 Fluids Engineering Division Summer Meeting
FEDSM2009
August 2-6, 2009, Vail, Colorado USA

FEDSM2009-78150

X-RAY PARTICLE TRACKING VELOCIMETRY IN FLUIDIZED BEDS

Joshua B. Drake[1], Lie Tang[2], and Theodore J. Heindel[1,*]
[1]Department of Mechanical Engineering
[2]Department of Agricultural and Biosystems Engineering
Iowa State University
Ames, Iowa 50011-2161

ABSTRACT

Fluidized beds are commonly found in the chemical and energy processing industries because of their low pressure drop, uniform temperature distribution, and high heat transfer rates. For example, in biomass gasification, biomass particles are injected into a heated bubbling bed of inert material (typically refractory sand) that volatilizes to form a flammable gas. However, the movement of the biomass particle through the bubbling bed is difficult to quantify because the systems are opaque. This paper describes X-ray particle tracking velocimetry (XPTV) applied to fluidized beds, where X-ray flow visualization is used to track the location of a single fabricated tracer particle as a function of time in a fluidized bed to study the bed/particle hydrodynamics. Using stereoscopic X-ray imaging, the 3D position of the tracer particle as a function of time is determined, from which tracer particle velocity can be calculated. Details and challenges of the XPTV process are also summarized.

Keywords: fluidized bed, particle tracking, stereography, X-rays, X-ray Particle Tracking Velocimetry

INTRODUCTION

Fluidized bed reactors have proven to be useful for various processes such as mixing, drying, fast pyrolysis, and catalytic cracking because they have the ability to provide a low pressure drop, uniform temperature distribution, and high heat/mass transfer rates [1]. These properties are due to circulation of the bed material by large voids of interstitial gas (i.e., bubbles). To improve the design and scale up in industrial applications, an understanding of the dynamic gas-particle and particle-particle behaviors is required. While flow patterns inside the bed are known to significantly affect flow behavior, the study of the bed hydrodynamics is problematic at best and, at times, impossible [2].

Fluidized bed hydrodynamics can be observed and quantified by invasive or noninvasive methods. Invasive investigative techniques use probes, such as protruding thermocouples that impede flow, potentially influencing data acquisition [3]. Goldschmidt et al. [4] have shown that noninvasive optical methods can be used in a thin rectangular fluidized bed reactor. However, more generalized reactor geometries make visual observation more difficult to implement because of the opaque nature of the reactor and bed materials. Therefore, visual methods are generally not effective unless the reactor is transparent and the region of interest is adjacent to the reactor walls [2]. Noninvasive techniques such as X-ray absorption, γ-ray absorption, or positron emission tomography utilize the ability to penetrate and/or pass radiation through dense and/or opaque materials alleviating the problems with visible techniques. Though similar to visible light, these techniques have the ability to visualize flow patterns through the opaque materials found in fluidized beds [5]. However, safety, expense, and limited resolution provide challenges for the implementation of these methods.

Limited research has been completed to reconstruct 3D velocity fields using radiographic methods. Guezennec et. al. [6] referenced many prior works in an effort to find the most efficient algorithms to automate the tracking of particles in turbulent flows. Kertzscher et. al. [7] and Seeger et. al. [8] have been perfecting an automated X-ray particle tracking velocimetry (XPTV) method for multiphase flows. An X-ray phase contrasting technique to visualize flows with large particle size disparities at great concentrations was implemented by Im et. al. [9]. Kim and Lee [10, 11] used

*Corresponding author, Phone: 515-294-0057; Email: theindel@iastate.edu

diffraction at the edges of particles to enhance detection at the microscale when quantifying velocity fields for a blood cell tracking method. An artificial neural network has also been suggested to automate the tracking of large concentrations of particles by XPTV with the intent of reconstructing 3D velocity fields [10, 11].

This study noninvasively observed, through the use of XPTV, the movement of a single tracer particle approximating a large piece of biomass injected into a cold flow fluidized bed. These observations led to a deeper understanding of the hydrodynamics of a cold flow gas-solid fluidized bed. The simulated biomass particle is tracked through the bed providing particle locations as a function of time.

EXPERIMENTAL PROCEDURES

Fluidized Bed Reactor

A schematic of the fluidized bed reactor is shown in Figure 1. It is fabricated from a 15.24 cm internal diameter clear acrylic tube with a 1.5 mm thick stainless steel aeration plate inserted between the plenum and bed chamber. The aeration plate contains 132 1 mm diameter holes drilled in concentric circles giving the aeration plate an open area ratio of 0.57%. Air is introduced into the system by an inlet in the bottom of the plenum, which is filled with glass marbles to evenly disperse the air over the bottom of the aeration plate. Rubber gaskets are placed between each flange, sealing the various components and forcing all gas to flow directly through the bed and out the top. A pressure tap in the bottom of the plenum holds a transducer connected to a computer controlled data acquisition card to record inlet pressure. A second tap on the side of the fluidized bed 3 cm above the aeration plate is used for particle and air injection. The reactor is placed precisely in the middle of the X-ray imaging facility and held firmly in place by a pair of C-clamps to reduce column vibration.

Bed Materials

The fluidized bed material used in this study were glass beads with a diameter range from 500 - 600 μm and fell within the Geldart type-B classification [12]. Because of the relatively high X-ray attenuation characteristics of glass, crushed walnut shell and ground corncob may also be used since they have been shown to fluidize in a similar manner [13]. Particle size ranges were obtained by thorough sieving with a shaker unit, and the glass beads were washed to assure they were contamination free, providing the most accurate bulk density and bed weights.

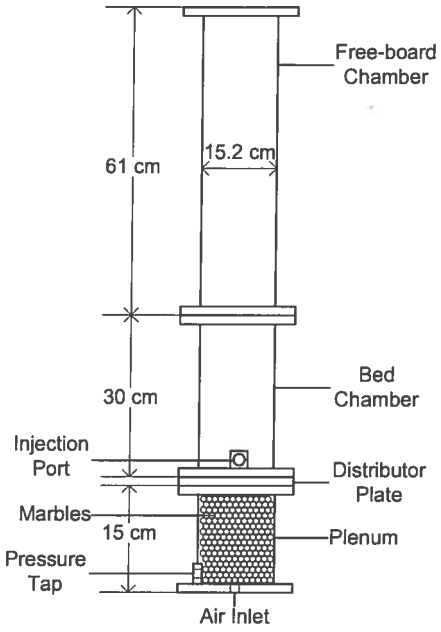

FIGURE 1: SCHEMATIC OF THE FLUIDIZED BED REACTOR.

X-ray Flow Visualization Facility

The X-ray flow visualization facility at Iowa State University has been described in detail elsewhere [14]; only a summary is described here. A dual source detector combination, mounted as shown in Figure 2, is used to produce the stereographic X-ray images. Each X-ray source is a LORAD LPX200 unit with adjustable voltage (10-200 KeV) and current (0.1-10 mA) capabilities. Images are produced using two identical Precise Optics PS164X 40.6 cm diameter image intensifiers and captured by two identical DVC1412 CCD cameras. These cameras are capable of capturing images at four spatial resolutions: 1388 × 1024 pixels, 640 × 512 pixels, 320 × 256 pixels, and 160 × 128 pixels. For the respective spatial resolutions, images can be captured at frame rates of 10, 20, 40, and 60 frames per second. In this study, the spatial resolution was set to 640 × 512, corresponding to a frame rate of 20 frames per second.

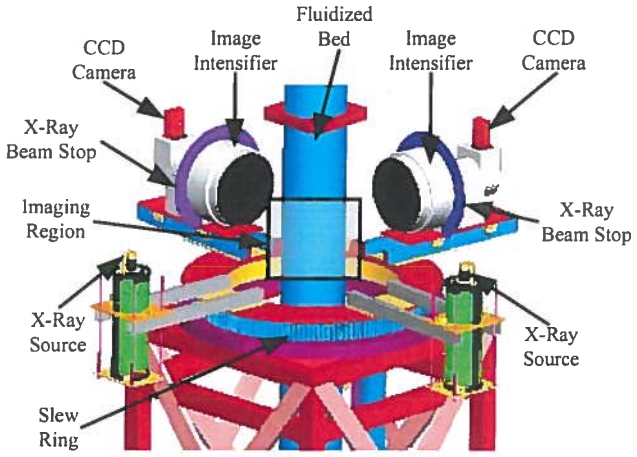

FIGURE 2: SCHEMATIC OF THE X-RAY FLOW VISUALIZATION FACILITY

Particle Injection System

The particle injection system is designed to inject a single particle into a fluidized bed at a desired time. It is similar to the design presented by Bruni et. al. [15] which involves a pneumatic actuator that pushes tracer particles directly into the bed. In the current study, it is desired to directly inject the particle into the bed using compressed gas. The gas injection also simulates the immediate volatilization of biomass as it is injected into the fluidized bed. Pneumatic systems are preferred over hydraulic and electromechanical systems since compressed air is readily available in the laboratory and a long actuator system is removed from the imaging region. Also, since the injector must be in close proximity to the reactor, and the fluidized bed is imaged with harmful ionizing X-rays, remote activation of the injector is required. In addition, the system is desired to maintain constant pressure to reduce the possibility of backflow.

Figure 3 shows a schematic of the single particle injection system. Tracer particles are stacked in a single vertical column in the hopper (b). The hopper is made of 1.04 cm ID copper pipe for rigidity and strength. Gravity is used to feed particles to the tee. The top of the hopper is plugged with a tube plug fitting (c) in order to maintain pressure in the injection system. A double-acting pneumatic cylinder provides the initial motion for particle injection. Since the cylinder is double-acting, it relies on compressed air to extend and retract the shaft. Two sections of polypropylene tubing supply the compressed air to the cylinder.

To inject a particle, the cylinder extends through the first tee where it contacts a particle and pushes it from the hopper to the center of the second tee. Compressed gas is supplied to the second tee which forces the tracer particle to travel into the injection tube. A combination of pressurized gas and gravity accelerates the tracer particle through the injection tube until it emerges in the fluidized bed (d) by way of the injector port (f).

After particle injection, the cylinder is retracted to prime the system for the next injection event. Because of the tight 0.07 cm tolerance between the cylinder rod and the copper tubing, additional tracer particles do not leave the hopper until the cylinder is retracted. Consequently, only one particle at a time is injected into the system. The injection system is controlled with two-way toggle switches which allow for remote control of the injection system; this is necessary since the injector board is located in the X-ray flow visualization facility and is inaccessible during X-ray operation.

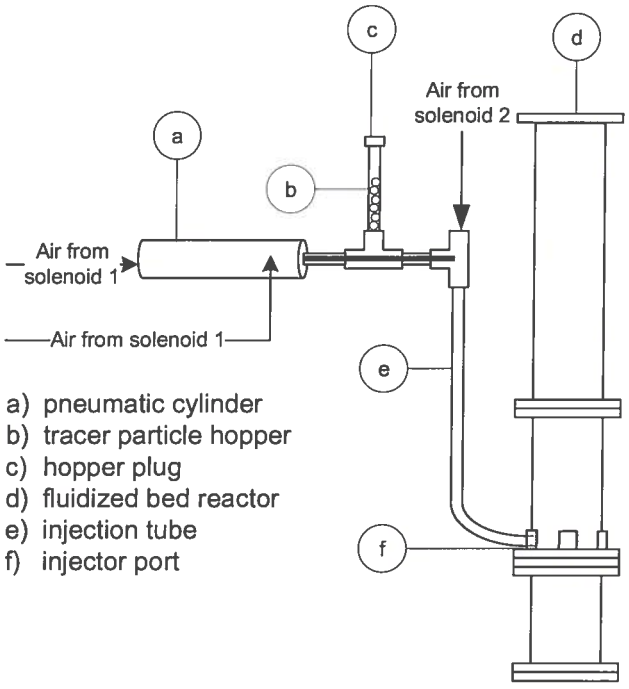

FIGURE 3: SCHEMATIC OF PARTICLE INJECTION SYSTEM.

XPTV IMAGING

XPTV Considerations

X-rays are produced by ionizing a target metal through bombardment of electrons, called a target source. These X-rays penetrate a target object as their intensity is attenuated based on that object's density and thickness. As either density or thickness increase, attenuation increases. An X-ray detector then records the attenuated X-ray intensity. If the detector is 2D, and the X-ray source produces a cone beam, a 2D projection of a 3D object is recorded, similar to a shadow image. One type of detector, called an image intensifier, collects the X-ray photons that fall onto it and converts them to electrons. The electrons are focused (intensified) onto a small region in which a CCD camera is used to capture an image called a radiograph.

XPTV, like particle image velocimetry (PIV), uses multiple images of a particle seeded flow to track particle motion as a function of time. However, unlike PIV particles, which only need to be small, neutrally buoyant, and absorb/reflect visible light, ideal XPTV particles must be small, neutrally buoyant, and attenuate X-rays. Since differential X-ray attenuation results primarily from density differences, a neutrally buoyant, differentially X-ray attenuating particle does not exist. To resolve this, most particles in XPTV systems are designed such that the desired effective density is produced with a composite particle; this particle is manufactured by combining a lighter material with a heavier, X-ray absorbing material. However, in doing this, most XPTV particles are typically much larger than PIV particles.

Unfortunately, not all bed materials have low X-ray attenuation characteristics. In a cylindrical fluidized bed reactor, X-rays will attenuate less near the walls, due to less material or a less dense path, and more in the center, due to more material or a more dense path. Consequently, even if an XPTV particle were highly absorbing, it still might not be seen when positioned in the center of the reactor because of contrast drowning or small differences in contrast between the bed and the particle. For particles to be good X-ray attenuators, a large quantity of the particle material must have an atomic number much greater than that of the bed medium. This material will be heavier than the bed medium, causing difficulties in manufacturing neutrally buoyant particles that stand out in dynamic imaging. A simple solution to the problem of contrast drowning is to increase the X-ray power settings; however, this could over saturate the wall regions of the fluidized bed causing a loss of contrast in this region of the image.

Tracer Particles in this Study

Because of the nature of X-rays and the fluidized bed characteristics, the tracer particle must be individually tailored to the system of interest. The tracer particle used in this study was manufactured with a two part urethane foam coating a semi-spherical tin/copper/selenium solder core (Figure 4). The foam coating and solder core were semi-uniformly shaped while the core was fairly centered inside the foam. Unintended irregularities caused the particle to have unstable moments of inertia and therefore tumbled while moving inside the dynamic bed better simulating a biomass particle. The particle was much larger than the bed material with a much smaller effective density to simulate an unvolitized biomass particle in a fluidized bed gasification unit. The particle weighs 0.35 g and displaced ~1.75 mL of water for an effective approximate density of 0.2 g/cm^3. This effective density is similar to softwood biomass that would be used as a feed stock in a fluidized bed gasification unit [16].

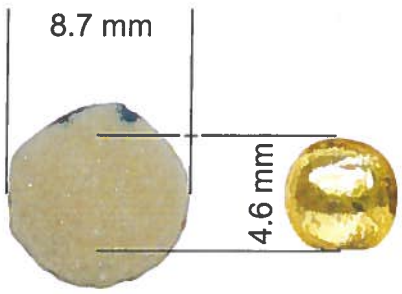

FIGURE 4: PICTURE OF THE COMPOSITE TRACER PARTICLE (LEFT). A SIMILAR TIN/COPPER/SELENIUM SOLDER CORE (RIGHT) IS IN THE CENTER OF THE COMPOSITE TRACER PARTICLE.

Automated XPTV

Radiographic images result from the single X-ray projection of a 3D object or process. Stereographic imaging is the process of capturing object projections from two independent directions (i.e., from two radiographs taken from two different projections, but acquired at the same instant in time). This method can be used to determine the correct 3D position of the object in space relative to a reference point. If the object of interest is dynamic, time-lapse images of the object are acquired to determine displacement between frames. In the case of XPTV, sequential images are digitized and stored for post processing. Prior to image acquisition, the X-ray system must be properly calibrated for pixel normalization, image unwarping, and beam hardening corrections, all of which are described elsewhere [14].

Because of the nature of X-rays and how they are detected visually, stereographic images are necessarily digitized in gray-scale. The tracer particle core absorbs more X-ray energy than the bed material creating a darker "shadow." Locating this sometimes subtle gradient with the naked eye is a learned task and, therefore, becomes easier to find through repetition. However, it becomes very time consuming if the number of images is very large. Using computer vision with a normalized cross-correlation (NCC) template matching detection method is an efficient solution for process automation [17]. This algorithm consists of calculating a correlation at each position of a search area within an image to measure the degree of similarity, or dissimilarity, between a given template and the current image subwindow [18]. The algorithm used in this study was written and tested in Matlab.

Once stereographic images of the dynamic fluidized bed have been acquired, normalized, and unwarped (see [14] for details), a region of interest (ROI) in the image is identified (i.e., the fluidized bed region). This is done manually and remains constant for all subsequent images. An X-ray radiographic image of the tracer particle is taken with each detector using the same power settings as those used in

acquiring the stereographic images. The tracer particle image then undergoes normalization, unwarping procedures.

The template vector, ω of size m × n pixels, is compared with each stereographic image region of the same size at every location. NCC-based template matching locates ω in each stereographic image, *I*, by searching for the maximum NCC function result. Let the center of ω in *I* be located at (*x*,y) and the region of *I* that the template covers be the search vector ω'. The NCC function can then be written as [17]

$$C(x,y) = \frac{\omega_n \cdot \omega'_n}{\| \omega_n \| \cdot \| \omega'_n |} \quad (1)$$

where both ω_n ω and ω'_n are normalized with means of zero and defined as:

$$\omega_n = \omega - \overline{\omega} \quad (2)$$

$$\omega'_n = \omega' - \overline{\omega'} \quad (3)$$

where $\overline{\omega}$ and $\overline{\omega'}$ are vectors of dimension $P = m\ x\ n$ and calculated in the following way:

$$\overline{\omega} = \frac{1}{p}\sum_{i=1}^{p} \omega_i \cdot \begin{bmatrix}1\\ \vdots \\ 1\end{bmatrix}^{p\times 1} \quad (4)$$

$$\overline{\omega'} = \frac{1}{p}\sum_{i=1}^{p} \omega'_i \cdot \begin{bmatrix}1\\ \vdots \\ 1\end{bmatrix}^{p\times 1} \quad (5)$$

The value of $C(x,y)$ is between -1 to 1 and reaches a maximum when the image intensity profiles of each vector are related by an affine transformation $A'=A\lambda+\mu$ for arbitrary constants λ and μ where λ>0. The affine transformation function allows for strong correlation base matching between two images when they is a change of intensity level [17]. The correlation function calculates the cosine of the angle between ω_n and ω'_n or the linear relationship between the vectors. The approximate spatial location of the tracer particle centroid can be calculated within each stereographic image. The location of the maximum value, C_{max}, indicates the spatial location of the particle centroid in the image matrix, *I*. Figure 5 shows the location of C_{max}, indicated in the right image by the red circle surrounding a bright spot. The left image, the blue circle surrounding the dark spot, indicates the particle. Using the particle centroid in each of this and subsequent images, both 2D and 3D instantaneous velocities and accelerations of the particle can be calculated.

Template Selection

The choice of particle template in this study was made by imaging a set of candidate particles. The candidate with a solder core that had the most uniform shape was chosen. Figure 6 shows the template chosen for this study. As can be seen, particle 1 had the most uniformly shaped core. The actual 16x17 pixel template is blown up and given a false color. A blue disk, indicating the particles solder core, is surrounded by a yellow-green halo, indicating the foam surrounding the solder core. The importance of the uniformity of both the halo and disk will be discussed in a subsequent section.

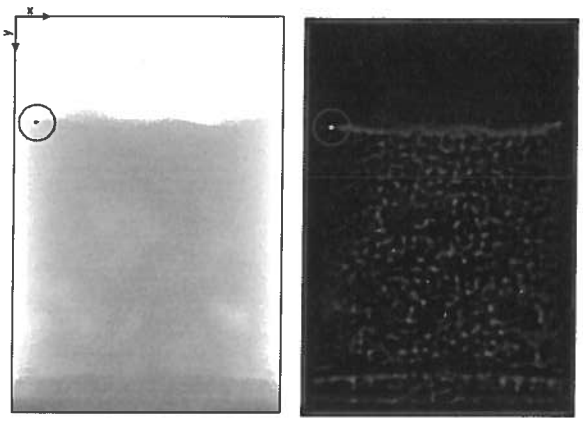

FIGURE 5: COMPARISON OF PARTICLE SPATIAL LOCATION IN A SINGLE RADIOGRAPHIC IMAGE (LEFT) AND THE RESULTING NCC MATRIX (RIGHT).

RESULTS

For this study, 260 images from each projection were acquired at a frame rate of 20 frames per second, covering 13 seconds of operation time. Because the time series of images from each detector needed to be analyzed separately, the percentage of successful hits per detector was different. The automated detection system gives a calculated particle centroid location for both x-z and y-z projections. If this location can be estimated visually in 1 projection and is approximately the same as the predicted location for the same projection, it is defined as a successful hit for that projection. The percentage of successful hits for detectors 1 and 2 were 91.5% (238/260) and 81.9% (213/260) respectively. Out of all unsuccessful hits for both detectors, only 12 occurred when the particle was not found in both x-z and y-z projections during the same instant in time.

The simple XPTV results shown here were acquired in a 15.2 cm ID fluidized bed filled with 500 - 600 μm diameter glass beads as the bulk media. The superficial gas velocity was quickly ramped up from U_g = 0 cm/s to U_g = 29.3 cm/s or 1.5 times the minimum fluidization velocity, U_{mf} [20]. A particle was injected into the fluidized bed after it reached quasi-steady state. Figure 7 shows sample stereographic projections, acquired from t = 3.45 s to t = 3.85 s, or over 0.40 seconds of tracer particle movement, although the discussion that follows includes 13 seconds of actual particle motion. At each time interval both the x-z and y-z projections are shown with the particle indicated by a red dot. Planar coordinate origins are show in each projection by red axis and black labels. This figure shows at time t = 3.45 s, the tracer particle lies ~10.7 cm above the aeration plate and ~2 cm from the wall radially.

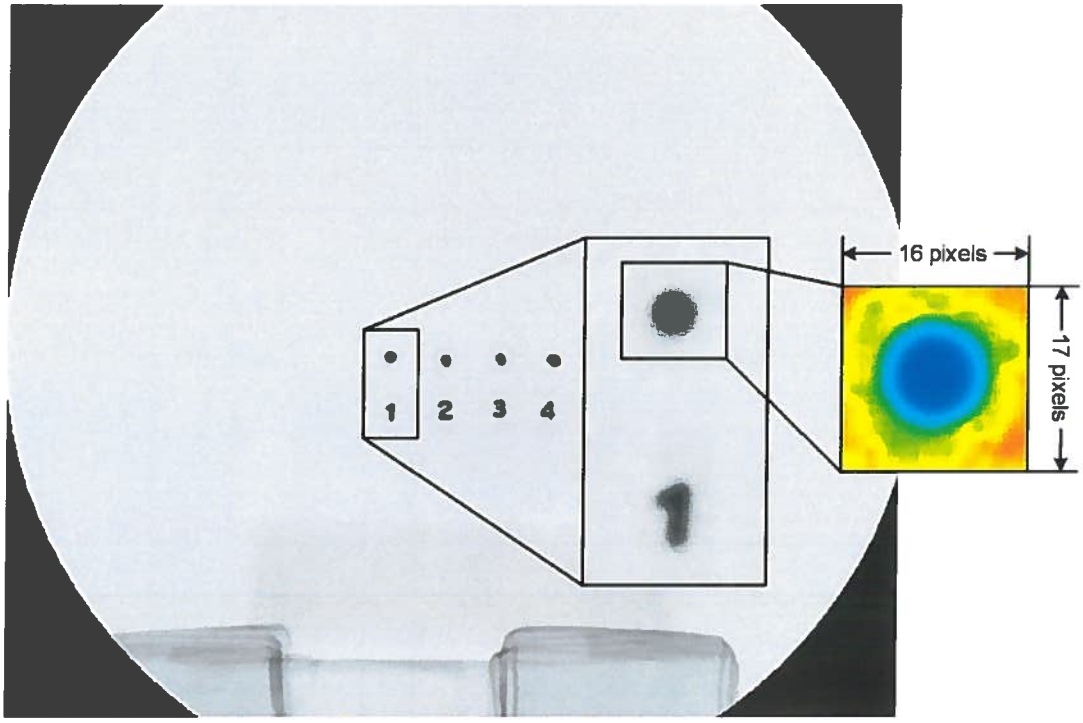

FIGURE 6: RADIOGRAPHIC IMAGE OF POSSIBLE PARTICLE CANDIDATES WITH A BLOW UP FALSE COLOR TEMPLATE IMAGE OF THE CHOSEN CANDIDATE.

From the sequential projections, it is observed that the particle initially travels slowly upward. The tracer particle movement is the result of a small bubble traveling up the wall under the particle (the lighter regions in each projection are regions of high gas content, i.e., gas bubbles). The bubble movement displaces bed material directly under the particle, displacing it as well. As the bubble overtakes the particle and encapsulates it, the particle falls through to the bottom of the bubble. There is not much horizontal movement of the particle, indicating that the bed material is circulating in the vertical direction at the tracer particle location. As time increases from t = 3.65 s to t = 3.85 s, the particle falls through 2 more bubbles.

Figure 8 graphs (a) and (b) show the tracer particles horizontal x- and y-displacements, respectively. In each figure, correctly identified particle positions from the automated process are shown with solid black circles and incorrect identifications are shown by solid red circles. Solid black lines drawn across the graphs at positions 7.62 cm and -7.62 cm designate the inside reactor wall boundaries. A dashed black line drawn across the graph at position 0 cm denotes the reactor center.

Although it may appear from Figure 7 that bubbles have little effect on the tracer particle horizontal movement, it can be seen in Figure 8 graphs (a) and (b) that there is significant horizontal movement when a longer time series is analyzed. This is a result of high inertial bed material being pushed by rising gas bubbles. The thickness and density of bed material particles that make up the surface of a bubble as it rises increases as the rise velocity increases. Therefore, a large fast rising bubble will have a thicker particle surface layer. The thicker the surface, the more momentum it has, so as the bubble rises, if it is incident on the tracer particle, it will transfer more momentum. This will move the particle more than that of a smaller slowly rising bubble.

At t = 0 s, the particle is approximately half way between the wall and reactor center. As bubbles coalesce, they become larger and rise faster, this in turn pushes bed material faster. If the particle is on the side of a rising bubble it will be pushed horizontally, which can be seen in Figure 8 between times t = 0 s and t = 2 s. Here most horizontal movement was in the x-direction.

In general the particle migrates away from the reactor center in the x-direction until about t = 6 s. However, in the y-direction the particle constantly moves towards the center. This indicates that for this fluidized bed reactor and experimental conditions, bubble coalescence and migration may not occur in the reactor center. This is because at lower U_g, jetting strength across the aeration plate may not be uniform [21]. Therefore, jets on one side may be stronger than the opposite side. Certain aeration holes may not be active as

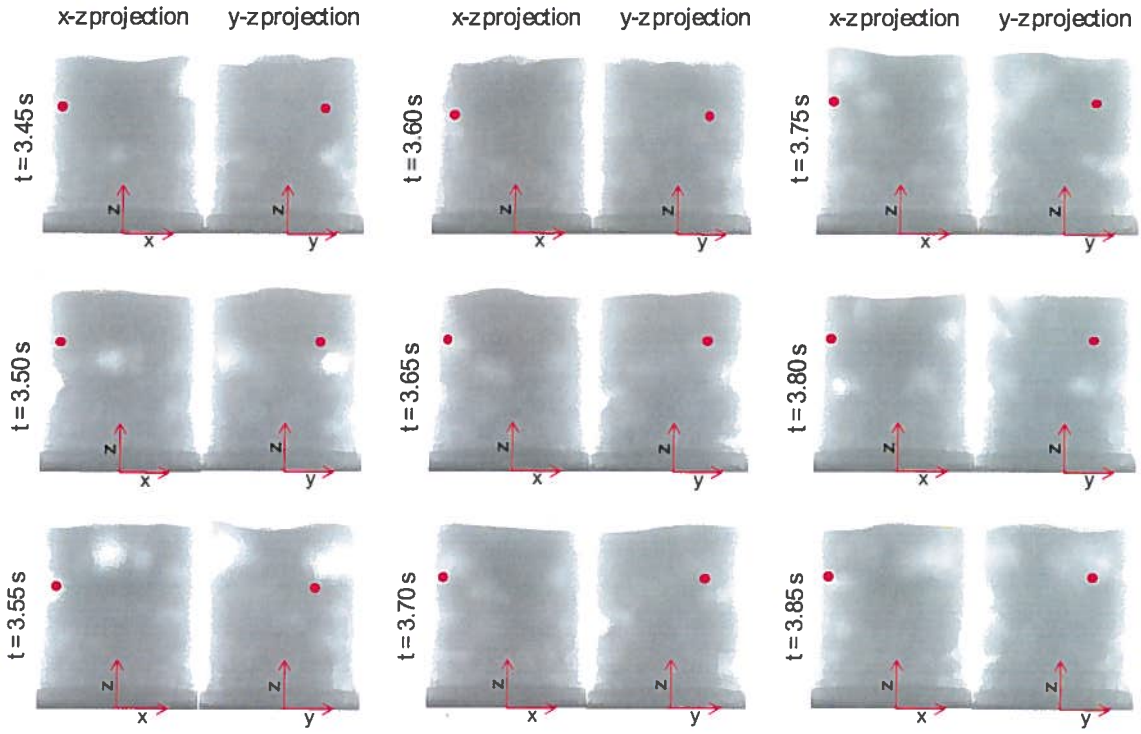

FIGURE 7: TRACER PARTICLE LOCATION IN A GLASS BEAD FLUIDIZED BED WITH U_g = 1.5 U_{mf}

well, creating greater bubble coalescence in areas where stronger jetting occurs. Figure 7 shows most bubbles appear to rise along the reactor walls, meaning recirculation of bed material may be greater in the reactor center. However, this could be misleading because the path length that X-rays travel through near the reactor walls is shorter than those passing through the center, causing an image saturation effect where not all bubbles can be detected or followed near the center for this X-ray power setting.

Figure 8 graph (c) shows the vertical positions of the particle over time. A solid black line at position 15.24 cm indicates the top of the static bed. Correct and incorrect particle locations are indicated the same as those in graphs (a) and (b). Three locations on this graph show points where possible jetting affects the particle movement drastically.

The tracer particle movement in the z-direction is much more cyclic in that it tends to follow the possible circulation pattern of bed material or rising bubbles. As can be seen in Figure 8, the particle initially travels toward the top of the bed then begins to fall. At $U_g = 1.5U_{mf}$ it is qualitatively observed in Figure 7 that more bubbles tend to rise along the walls creating a bubbling zone. As the bubbles rise, bed material is entrained and carried to the top of the bed then disengages as the bubble erupts from the top. The material then is possibly recirculated down through the reactor center, called the recirculation zone. If the particle is on the edge of these two zones then the rising bubbles will push the particle into the recirculation zone where it becomes entrained and is drawn down toward the bottom of the bed. As the particle reaches a low point in the bed, it is abruptly pushed upward. This is because of jetting gas coalescing into bubbles causing some bed material to circulate up to the top of the bed. Figure 8 graph (c) shows 3 cycles of this phenomenon where the particle reaches a local minimum then travels back to the top of the bed. The local minimum appears to occur at approximately the same location; however, just after the third cycle the particle begins to fall to the bottom of the bed. At this point the particle falls between the jets and is no longer affected by the recircualting bed material. This is because the material between the jets does not move which is evident from very little horizontal movement of the particle at this point (see Figures 8 graphs (a) and (b)). The small amount of horizontal particle movement in the y-direction at the bottom of the bed is most likely due to aeration jets increasing and decreasing in strength or it is bouncing between jets.

The aeration plate that distributes gas into the bed, although uniformly distributed with holes, may not behave uniformly at this U_g. Hence, not all holes are active at a given instant in time creating uneven jetting patterns. This phenomena can be seen in computed tomography images of a similar bed [21, 22].

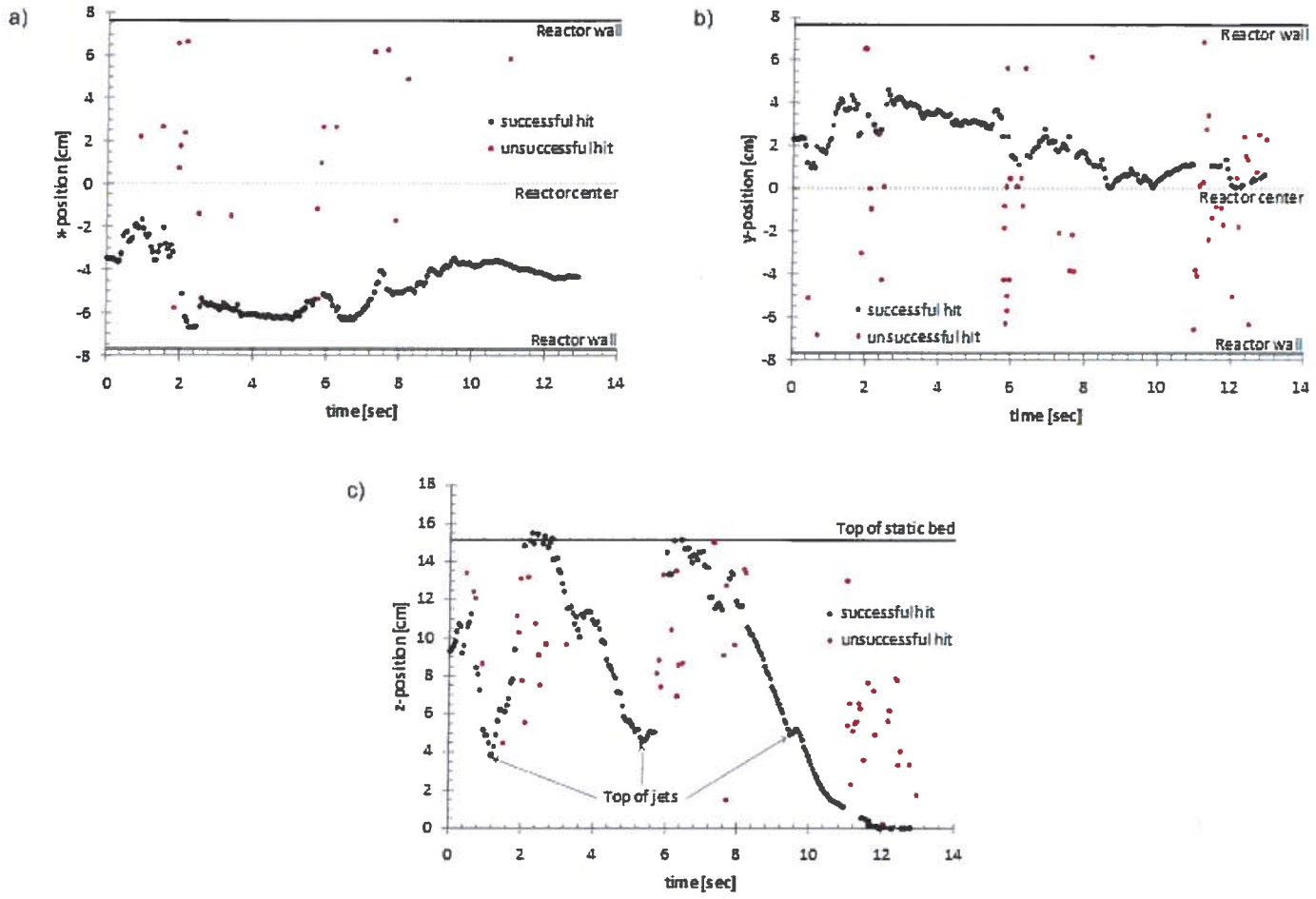

FIGURE 8: GRAPHS OF THE (a) X-, (b) Y-, AND (c) Z- PARTICLE POSITIONS VS. TIME

XPTV IMPROVEMENTS

The automation of particle detection is only as strong as its efficiency and accuracy. This study only processed 520 images in ~25 seconds using Matlab R2008a on a Dell Precision 7200 workstation with 2 2.6 GHz 3400 Intel quad-core processors. The computation time is a function of image quantity, image size, computational speed of the computer, and programming practices. These parameters can be optimized for higher performance of the detection system.

The speed of particle detection can be improved dramatically by reducing the search area within the dynamic stereographic images. This can be done by finding four successive images in the series where the particle can be identified successfully. An instantaneous particle velocity and acceleration can then be determined between images 1 and 2, 2 and 3, and 3 and 4. These three velocities and two accelerations can be compared to find a general direction and displacement of the particle in the bed. By using the difference in the change in direction of the particle from image to image, the search box center and size can be calculated. NCC matching would be calculated for this search box to find the particle. This technique would only be successful if the particle movement in the bed was not very erratic or fast.

If the prior method is suitable for detection, then a system for testing if the particle was found properly should be used. Knowing this, the predicted particle position should indicate the center of the particle. A ROI centered on this location with the same size as the particle template is taken from the stereographic image being analyzed. An array of images the size as this ROI including all neighbors in a 5×5 grid around the predicted particle ROI is created (see Figure 9). The texture of each neighbor image in the array is calculated and tested against the predicted particle region. Although not implemented in this study, the method of testing the predicted

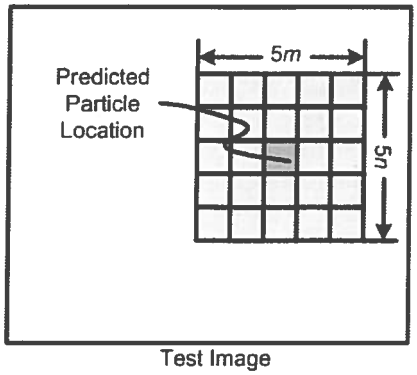

FIGURE 9: IMAGE ARRAY SURROUNDING THE PREDICTED PARTICLE LOCATION IN A TEST IMAGE.

particle was attempted. It was found that the standard deviation, skewness of the histogram, uniformity, and entropy of each region were good statistical tests of the predicted particle position. The calculation and importance of these statistics are explained by Gonzalez et al. [23]. In fact, this test was able to properly identify those predictions that were previously incorrect 62.5% of the time; however, the amount of incorrectly identified predictions was 36% when applied to all images.

Another test can be used to help find the particle location in an image projection that is incorrectly identified by using the correctly identified position in the perpendicular projection acquired by the other detector. Because both images were acquired at the same time, the z-position of the particle in one image should be the same in the other. This height becomes the center of an ROI including all pixels across the incorrectly identified image and bounded by two times the height of the template. This ROI would go through NCC matching and checked with the previous method for accuracy.

Lastly, physical acquisition of the dynamic system could be improved by increasing the frame rate. For this study it was observed that at superficial gas velocities greater than $U_g = 1.5U_{mf}$, the successful hit rate decreased drastically. As U_g increased, the velocity of the particle increased and therefore was blurred in subsequent images. The blur is in the form of streaking, creating particle regions in the image that are unable to be correlated with template matching. As stated previously, the uniformity of the halo and central disk in the template image gave a higher percentage of correct particle location predictions than if only the core was chosen for the template. The larger and more uniform the intensity profile of the template, the better the correlation with the particle image. For this study the frame rate could not be increased without a loss in spatial resolution; therefore, faster cameras could be useful in future studies.

CONCLUSIONS

This study shows that a particle used to simulate unvolitized biomass in a fluidized bed gasification unit possibly moves along the lines of recirculating bed material, or falls through or is pushed by rising bubbles. Bubble surfaces play a significant role in particle movement in the bed through inertial forces. Jetting close to the aeration plate was important in keeping the particle aloft in the bed; however, the particle eventually became inactive because of uneven jetting due to aeration plate design. The acquisition system could be improved, yet proved to be valuable in obtaining non-destructively 3D position data about a particle in an opaque dynamic system.

ACKNOWLEDGEMENTS

The X-ray facility used in this research was funded by the National Science Foundation under award number CTS-0216367 and Iowa State University. Partial support for the work described in this paper from the ConocoPhillips Company is acknowledged.

REFERENCES

[1] Crowe, C.T., *Multiphase Flow Handbook.* 2006, Boca Raton, FL: CRC Press.

[2] Drake, J.B., Franka, N.P., and Heindel, T.J. "X-Ray Particle Tracking Velocimetry for Applications in Fluidized Beds." in *ASME International Mechanical Engineering Congress and Exposition*. 2008. Boston, MA, USA: ASME

[3] Tavoularis, S., *Measurements in Fluid Mechanics*. 2005, Cambridge, NY: Cambridge University Press. 354.

[4] Goldschmidt, M.J.V., Link, J.M., Mellema, S., and Kuipers, J.A.M., "Digital Image Analysis Measurements of Bed Expansion and Segregation Dynamics in Dense Gas-Fluidised Beds," *Powder Technology*, 2003. **138**(2-3): p. 135-159.

[5] Hilal, N., Ghannam, M.T., and Anabtawi, M.Z., "Effect of Bed Diameter, Distributor and Inserts on Minimum Fluidization Velocity," *Chemical Engineering and Technology*, 2001. **24**(2): p. 161-165.

[6] Guezennec, Y.G., Brodkey, R.S., Trigui, N., and Kent, J.C., "Algorithms for Fully Automated Three-Dimensional Particle

Tracking Velocimetry," *Experiments in Fluids*, 1994. **17**(4): p. 209-219.

[7] Kertzscher, U., Seeger, A., Affeld, K., Goubergrits, L., and Wellnhofer, E., "X-Ray Based Particle Tracking Velocimetry - a Measurement Technique for Multi-Phase Flows and Flows without Optical Access," *Flow Measurement and Instrumentation*, 2004. **15**(4): p. 199-206.

[8] Seeger, A., Affeld, K., Goubergrits, L., Kertzscher, U., and Wellnhofer, E., "X-Ray-Based Assessment of the Three-Dimensional Velocity of the Liquid Phase in a Bubble Column," *Experiments in Fluids*, 2001. **31**(2): p. 193-201.

[9] Im, K.-S., Fezzaa, K., Wang, Y.J., Liu, X., Wang, J., and Lai, M.C., "Particle Tracking Velocimetry Using Fast X-Ray Phase-Contrast Imaging," *Applied Physics Letters*, 2007. **90**(9): p. 091919.

[10] Lee, D.J. and Cha, S.S. "Three-Dimensional Measurement of Fluid Flow by Stereoscopic Tracking Velocimetry." in *Optical Technology and Image Processing for Fluids and Solids Diagnostics Proceedings*. 2003. Beijing, China: The International Society for Optical Engineering.

[11] Lee, D.J., Cha, S.S., and Ramachandran, N. "Three-Dimensional High-Resolution Optical/X-Ray Stereoscopic Tracking Velocimetry." in *ASME International Mechanical Engineering Congress and Exposition*. 2004. Anaheim, CA: ASME.

[12] Geldart, D., "Types of Gas Fluidization," *Powder Technology*, 1973. **7**(5): p. 285-292.

[13] Franka, N.P., Heindel, T.J., and Battaglia, F. "Visualizing Cold-Flow Fluidized Beds with X-Rays." in *ASME International Mechanical Engineering Congress and Exposition*. 2007. Seattle, Washington: ASME.

[14] Heindel, T.J., Gray, J.N., and Jensen, T.C., "An X-Ray System for Visualizing Fluid Flows," *Flow Measurement and Instrumentation*, 2008. **19**(2): p. 67-78.

[15] Bruni, G., Solimene, R., Marzocchella, A., Salatino, P., Yates, J.G., Lettieri, P., and Fiorentino, M., "Self-Segregation of High-Volatile Fuel Particles During Devolatilization in a Fluidized Bed Reactor," *Powder Technology*, 2002. **128**(1): p. 11-21.

[16] Brown, R.C., *Biorenewable Resources Engineering New Products from Agriculture*, ed. Brown, R.C. 2003, Ames, IA: Blackwell Publishing. 286.

[17] Tang, L. and Tian, L.F., "Real-Time Crop Row Image Reconstruction for Automatic Emerged Corn Plant Spacing Measurement," *Transactions of the ASABE*, 2008. **51**(3): p. 1079-1087.

[18] Mattoccia, S., Tombari, F., and Di Stefano, L., "Fast Full-Search Equivalent Template Matching by Enhanced Bounded Correlation," *IEEE Transactions on Image Processing*, 2008. **17**(4): p. 528-538.

[19] Fisher, R., Perkins, S., Walker, A., and Wolfart, E. *Geometric Operations: Affine Transformation*. 2000 2003 [cited 2009 March 12]; Image Processing Learning Resources:[Available from: http://homepages.inf.ed.ac.uk/rbf/HIPR2/affine.htm.

[20] Franka, N.P., Drake, J.B., and Heindel, T.J. "Minimum Fluidization Velocity and Gas Holdup in Fluidized Beds with Side Port Air Injection." in *ASME Fluids Engineering Division Summer Meeting*. 2008. Jacksonville, Fl, USA: ASME.

[21] Franka, N.P. and Heindel, T.J., "Local Time-Averaged Gas Holdup in a Fluidized Bed with Side Air Injection Using X-Ray Computed Tomography," *Powder Technology, In Press*, 2009.

[22] Franka, N.P., *Visualizing Fluidized Beds with X-Rays*. M.S. Thesis. 2008, Ames, IA: Iowa State University.

[23] Gonzalez, R.C., Woods, R.E., and Eddins, S.L., *Digital Image Processing Using Matlab*. 2004, New Jersey: Pearson Prentice Hall.